MARINE ROBOTS

Autonomous seeking and mapping coral reef biodiversity hotspots with a multimodal AUV

Seth McCammon[1]*, Levi Cai[1,2], Daniel Yang[1,2], John Walsh[1], John D. Cast[1], T. Aran Mooney[3], Yogesh Girdhar[1]*

Coral reefs are under threat worldwide. Yet, in these often-challenging marine habitats, biologists lack the tools to quantify the spatial heterogeneity of mobile reef fauna at high resolution (<1 meter), hampering monitoring and restoration efforts. Because of the diverse species present, multiple sensor modalities are needed to characterize the biodiversity. The urgent need to expand this study across unexplored reefs worldwide compounds these challenges. To address these problems, we propose a generative model of reef observations and develop a multimodal framework for seeking and mapping hotspots of biodiversity. In a case study on a healthy Caribbean reef, our autonomous underwater vehicle used passive acoustics and visual sensing to locate a biological hotspot around a large *Dendrogyra* pillar coral. We used the colocated multimodal data to self-validate the hotspot's prominence, representing a technological step forward to help understand the ecological dynamics of coral reefs.

INTRODUCTION

Biodiversity is a key metric for quantifying the health of ecosystems worldwide, measuring the absolute and relative abundance of different species of organisms. However, this biodiversity is not uniformly distributed but instead clusters into "hotspots" or regions with notably higher density of diverse species (*1*, *2*). Initially, this hotspot model was used to describe whole ecosystems. However, more recent work has shown that this heterogeneity exists in a fractal pattern across all spatial scales in an ecosystem. Variability in factors such as availability of food or shelter can create spatial heterogeneity in the distribution of different species on the scale of kilometers (*3*) or even meters (*4*, *5*). Localizing these hotspots and assessing their density and extent is a challenging task, because it requires direct observations of many, vastly different species. Observing these different species necessitates an equally diverse array of sensors because survival adaptations, such as camouflage or hiding behaviors, may make some species all but invisible to any given sensing modality.

Here, we focus on the task of assessing biodiversity on coral reefs. Despite covering less than 0.01% of Earth's oceans (*6*, *7*), an estimated 25% of marine species spend some portion of their life cycle on a coral reef (*8*). Because of factors such as rising ocean temperatures, disease, overfishing, and coastal development, today's reefs are under threat globally (*9*–*11*). To maximize the effectiveness of conservation and restoration efforts and to better manage these resources under stress, there is a need to improve our ability to measure the spatial, temporal, and ecological heterogeneity of coral reefs. Within the boundary of a reef, hotspots exist at or below the meter scale (*4*, *5*). Traditional methods, such as diver-based surveys, are not designed to resolve these features beyond the scale of an entire reef, limiting the resolution of the data available to stakeholders and policy-makers. In contrast, autonomous underwater vehicles (AUVs) can produce maps of underwater benthic structure over larger areas with higher spatial resolution, up to the centimeter scale (*12*–*14*), and their ability to be equipped with many different sensors makes them an ideal choice for multimodal assessment of biodiversity. However, to date, these autonomous surveys have focused on the static benthic portion of coral reefs, ignoring or overlooking the dynamic fish and mobile invertebrate fauna that make up a major portion of the rich biodiversity of a coral reef.

The most commonly used method to study mobile species on coral reefs, such as pelagic fish, is through systematic surveys conducted by trained scientific scuba divers (*15*–*18*). These surveys typically collect visual data, recorded using a handheld camera or in situ counting of fish and coral. Analyses of these surveys average results over multiple transects and are not designed to provide assessments of spatial ecological heterogeneity. The scope of reef studies is limited by the high cost of training a scientific diver, the health risks associated with frequent dives (*19*), and the difficulty of accessing often-remote reefs. Consequently, only a small fraction of the world's reefs are surveyed, and those surveys occur no more than once or twice per year, covering only a small portion of the reef (*20*, *21*). In the past decade, another method for reef health assessment has emerged using passive acoustic monitoring (PAM) equipment on reefs to study the underwater soundscape (*22*–*25*) and sounds of animals. Given that the true number of soniferous species is unknown, it is believed that between 47% (*26*) and 71% (*27*) of fish species produce sounds (*28*). These sounds include intentional calls, such as those for territorial defense, attracting mates, and coordinating spawning (*29*, *30*), and incidental sounds, such as those during swimming, feeding, or photosynthesizing (*31*–*33*). These sounds can be detected over long ranges. Damselfish (*Dascyllus albisella*) calls can be detected at a range of 12 m with a signal-to-noise ratio of 5 to 10 dB (*34*). In quieter environments, these ranges can extend to upward of 50 m (*35*, *36*). In contrast, vision-based detection is limited to a few meters because of the effects of absorption, attenuation, and scattering (*37*, *38*). However, visual signals carry more information. For example, visual detection of fish species is commonplace (*39*–*41*), yet species identification remains out of reach for state-of-the-art acoustic detectors (*24*, *42*). Cryptic species, those that prefer to conceal themselves in the rocks and coral structure of a reef (*43*), are hidden to visual sensors. Relying exclusively on passive acoustic sensing will fail to detect organisms that do not vocalize (*44*) or otherwise

[1]Applied Ocean Physics and Engineering Department, Woods Hole Oceanographic Institution, Woods Hole, MA, USA. [2]MIT-WHOI Joint Program, Cambridge, MA, USA. [3]Biology Department, Woods Hole Oceanographic Institution, Woods Hole, MA, USA.
*Corresponding author. Email: smccammon@whoi.edu (S.M.); ygirdhar@whoi.edu (Y.G.)

produce sound. These factors provide a strong motivation for the use of multiple, overlapping sensing modalities to more accurately measure biological activity on coral reefs.

To address the scalability, cost, and risks involved with using divers on coral reefs, different methods for deploying mobile sensors on reefs have been investigated. Towed camera systems and remotely operated vehicles (ROVs) have also been used for visual surveys of reefs (*45*, *46*). However, ROVs require constant direct oversight, which limits scalability, and ROV tethers bound the range of operation and bring a risk of entanglement and damage to the reef (*47*). Towed camera systems can achieve faster coverage than an ROV or a diver; however, image quality can suffer, particularly on reefs where complex topography can heighten the principal challenges of towed camera deployments: maintaining constant altitude, avoiding collision with the reef, and ensuring that the camera remains perpendicular to the seafloor (*48*). AUVs have perhaps the greatest potential to be a scalable solution for studying dynamic organisms on coral reefs. Operating an AUV requires much less training than scientific diving while also mitigating risks to humans. Many coral reefs are shallow, making them accessible to smaller AUVs that are more affordable for conservationists and scientists. Now, AUVs are most often used to map static components of benthic substrates, including coral (*12*–*14*) and seagrass (*49*), using visual and inertial sensors to localize themselves (*50*, *51*) and to make large and high-quality maps of benthic substrates. Although these surveys may occasionally observe mobile organisms (*52*), the study of these organisms is not typically the focus. AUVs have been used to study mobile organisms; however, these methods have typically been developed for midwater applications, using active acoustics (*3*), acoustic tags (*53*), and visual tracking, without the clutter of the seafloor (*54*, *55*) and for larger organisms (*56*, *57*).

Here, we make two primary contributions (Movie 1). The first of these is an autonomy framework that consists of four hotspot discovery behaviors linked by a generative model of multimodal species observations on a coral reef as outlined in Fig. 1. This system addresses the needs of marine biologists for scalable tools capable of studying the distribution of biological activity on reefs with submeter-scale resolution across a wider variety of species than any sensing modality alone. Where there is overlap between visually and acoustically observable species, our system provides overlapping multimodal measurements that can self-validate the existence of hotspots, an important capability for exploring unknown reefs. The second major contribution of this work is a case study demonstrating the different behaviors in a set of overlapping experiments located on a healthy Caribbean reef. For this case study, we present data from three visits to Joel's Shoal reef, a model reef with high biodiversity in the US Virgin Islands (*58*, *59*), between November 2022 and March 2024. In these experiments, we used the four autonomous hotspot discovery behaviors to assess biological activity on the reef. We then show how the data from these missions can be used to make inferences about the unobservable ecological processes of the reef that drive hotspot formation. These experiments used our existing AUV system, Curious Underwater Robot for Ecosystem Exploration (CUREE) (*60*), whose unique combination of onboard computation and modular design (Fig. 2) allows it to support the multimodal adaptive missions presented here.

RESULTS

Hotspots of biological activity can be detected by estimating locations with high animal abundance. Our approach used complementary multimodal observations, specifically vision and passive acoustic sensing. By using these two modalities in both open- and closed-loop autonomous control, we developed four distinct hotspot discovery behaviors: a visual fish census, acoustic hotspot mapping, acoustic homing using biological signatures, and visual tracking of sentinel species. These behaviors were lined by a generative model that described how different types of observations of species distributions on coral reefs related to the presence and/or absence of hotspots. The behaviors could either be used in isolation or combined as building blocks for multimodal missions that allowed users to optimize around the trade-offs between sensing modalities and hotspot discovery strategies. To demonstrate this capability, we performed a series of experiments using our AUV, CUREE (*60*) (Fig. 2). These experiments were located at Joel's Shoal, an ecologically important reef on St. John (Fig. 3), between November 2022 and March 2024. A list of the individual AUV deployments that made up these experiments is provided in table S1.

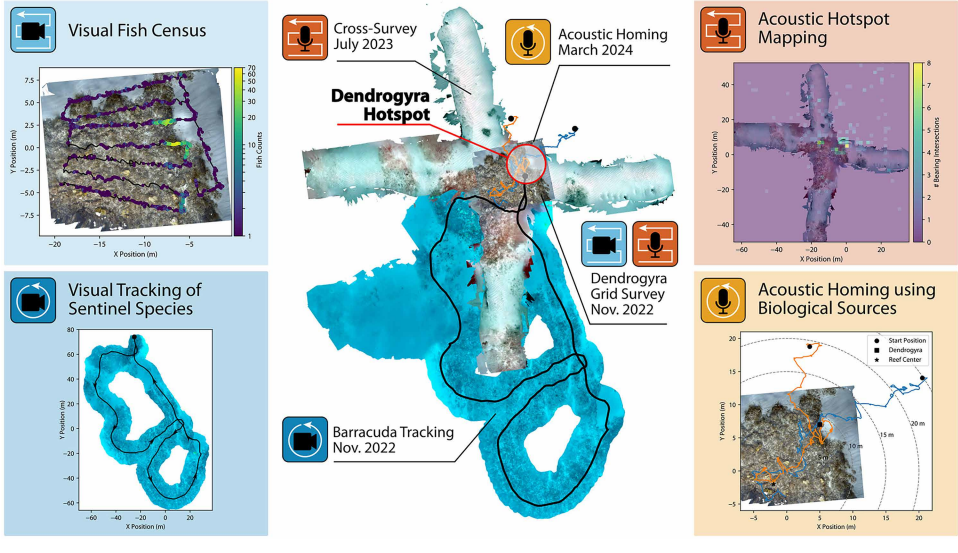

Movie 1. Overview of multimodal hotspot seeking and mapping behaviors. We show how two different sensing modalities, vision and passive acoustics, can be used in both an open-loop hotspot mapping behavior and a closed-loop hotspot seeking behavior. Using these behaviors, we were able to repeatedly identify the region around a *Dendrogyra* pillar coral as an active biological hotspot on a Caribbean coral reef.

Generative model of reef hotspots

The link between the robot's observations of the reef and the distributions of biological activity that produce those observations was formulated using the generative model shown in Fig. 1. In this model, each location on the reef has a set of underlying habitat characteristics, such as the rugosity, the local soundscape, or any number of other difficult-to-observe

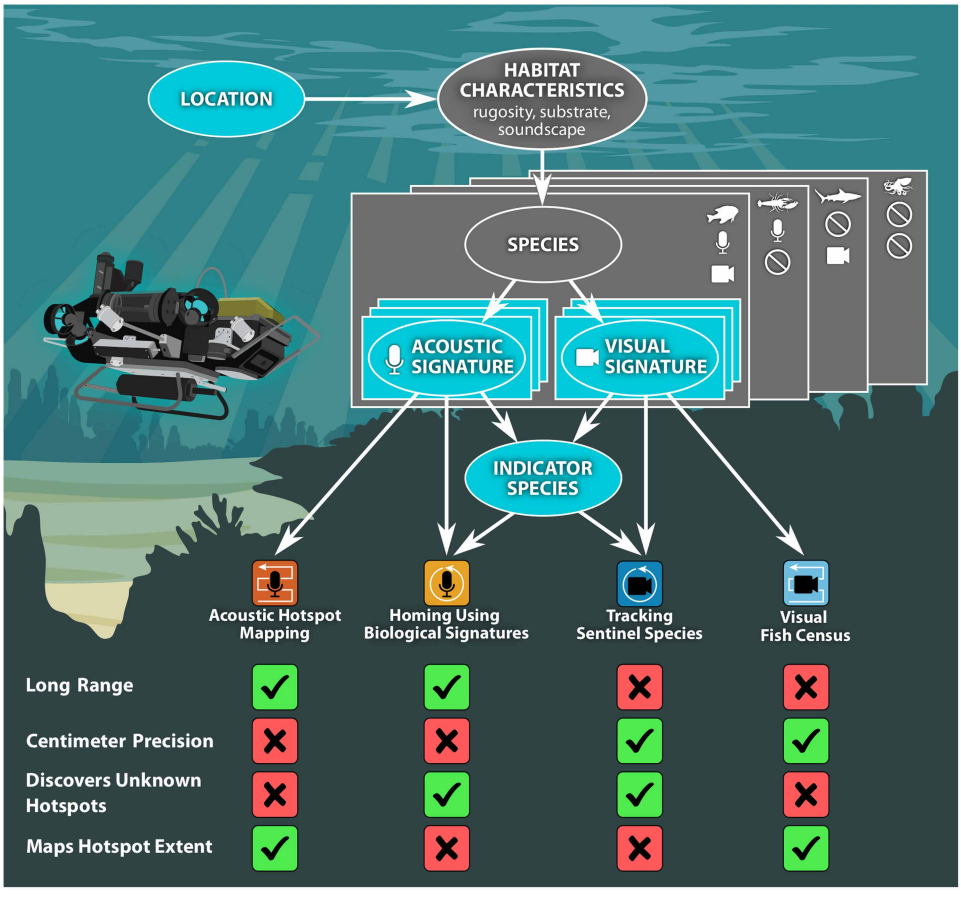

Fig. 1. Generative model for visual and acoustic observations of biological activity on a coral reef. The plate notation model (*97*) consists of nodes (ovals) that represent features in the environment. Plates (rectangles) group these nodes where there are multiple parallel instances, for example, multiple species on the reef or different appearances or sounds of a single species. Nodes are linked by causal relationships (arrows). The problem of detecting hotspots of biological activity can be formulated as estimating the locations that have the highest animal abundance. Our four hotspot discovery behaviors are designed to leverage observable environmental features (blue) while avoiding reliance on unobservable features (gray). Further study of datasets collected using these behaviors allows marine biologists to make inferences about unobserved features.

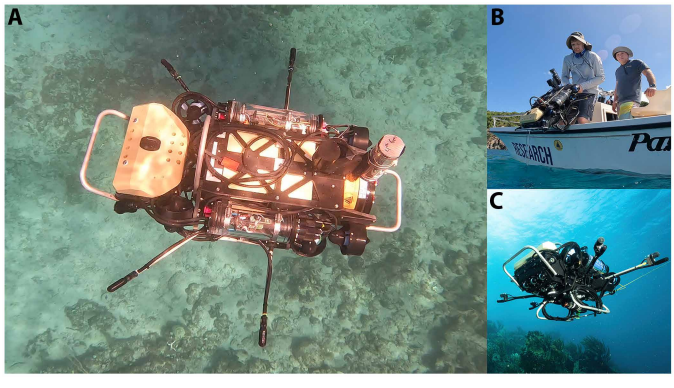

Fig. 2. CUREE. (**A**) CUREE is a small, portable AUV designed for autonomous exploration of shallow water ecosystems (*60*). (**B**) CUREE is easily deployed by a single person from a small boat. (**C**) Its multimodal sensing includes four hydrophones mounted on extended arms and forward- and downward-facing cameras to seek out hotspots of biological activity on coral reefs.

environmental processes (*61*). The cumulative effect of these factors combined with different species' preferences for each gives rise to a complex distribution of biological hotspots, H, across locations, X, on a reef, represented by the distribution $P(H, X)$. However, this distribution cannot be measured directly. Instead, our AUV made a set of observations $Z_{s,m}$, where s is the species or subset of species observable with a sensing modality m. Thus, the distribution of hotspots can be written as

$$P(H,X) \propto \sum_{m \in M} \sum_{s \in S} P\left(H|H_s\right) \times P\left(H_s|Z_{s,m}\right) \times P\left(Z_{s,m}|X\right) \quad (1)$$

where S is the set of species present on the reef and M is the set of sensing modalities available to the AUV. The first term, $P(H|H_s)$, contains the likelihood that a hotspot of a given species indicates a larger multispecies hotspot. The second term, $P(H_s|Z_{s,m})$, represents the "directness" of the observations of a species with a given sensing modality, equivalent to the sensor model in a partially observable Markov decision process (*62*). The last term, $P(Z_{s,m}|X)$, is the set of observations collected by the robot during a mission. Although we present this model in the context of studying coral reefs with an AUV, it generalizes to any multimodal exploration and mapping of sparse and heterogeneously distributed phenomena.

On a reef, the contribution of a species hotspot to overall biodiversity, $P(H|H_s)$, is typically unknown, and gathering data to better understand it is one of the biological objectives. In contrast, after a mission, the subset of the reef visited by the robot, $P(Z_{s,m}|X)$, is fully known. Thus, behavior design and sensor selection has the greatest effect on the scientific value of observations by shaping the directness distribution, $P(H_s|Z_{s,m})$.

Where the observation model is more direct, it is advantageous to use it with exhaustive, open-loop behaviors, because each $Z_{s,m}$ provides more information about H_s. However, this exhaustive mapping is typically not feasible to use to cover all $x \in X$ (although the greater range offered by acoustic observations helps offset this at the cost of directness), and so we also developed behaviors that can leverage less direct information that can be used to "warm start" the more direct mapping behaviors. Additionally, these behaviors can be used to find local maxima in the respective H_s for ecological assessments that do not require the full distributions. Acoustically, this presents itself as a simple gradient-following homing behavior. Visually, it leverages the knowledge and experience of an intermediary sentinel species to guide the AUV along the same gradient.

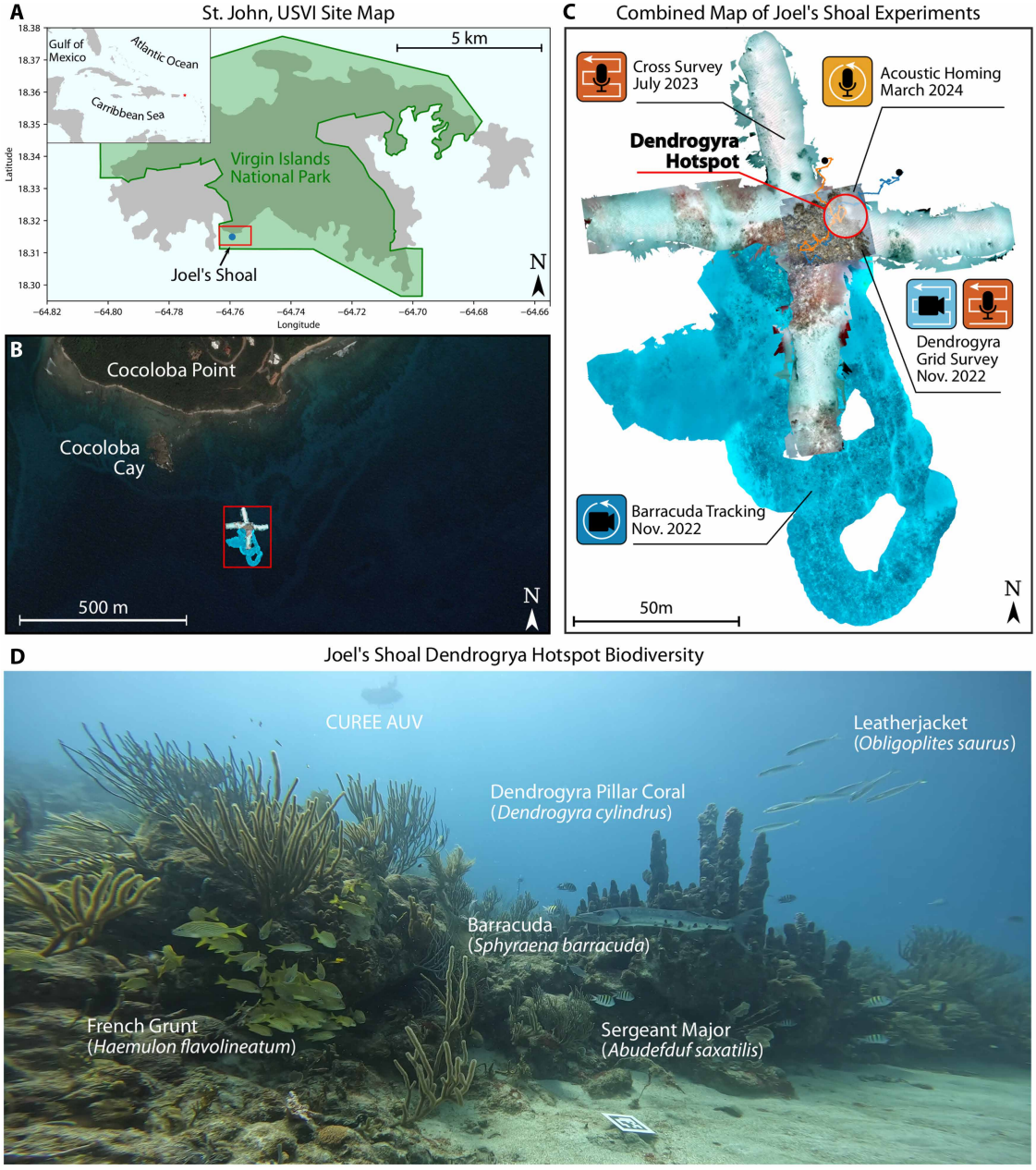

Fig. 3. Overview of the Joel's Shoal experiment site. (**A**) Joel's Shoal reef is located within the boundary of the Virgin Islands National Park near St. John in the US Virgin Islands (USVI). (**B**) The reef lies between 6 and 12 m deep, ~350 m south of Cocoloba Point. (**C**) Orthomosaics reconstructed over the four experiments to Joel's Shoal paint a complete picture of the reef and the sand flats that surround it. The reef consists of a rocky coral-covered region ~20 m by 30 m in size. The composite of individual orthomosaics was done manually. Individual orthomosaics are in the Supplementary Materials as figs. S1 to S3. (**D**) Joel's Shoal is an ecologically diverse site, and it hosts a wide range of fish species and coral.

Visual fish census

The first experiment that we conducted at Joel's Shoal was a visual fish census to produce a high-resolution map of the number of visible fish at each point on the reef. The census took a systematic approach to visual observation of a reef, collecting data similar to those of a human diver survey. However, the AUV's ability to localize itself underwater provided much better position estimates for systematically gridded data for high-resolution analysis. In our visual census, CUREE followed a back-and-forth lawnmower survey pattern (*63*) over a 15 m–by–20 m portion of Joel's Shoal, and it used downward- and forward-facing cameras to record fish and other organisms in the survey region for later analysis. In total, the survey took 33 min 19 s to complete, with a path length of 210.1 m. Runtime and distance information for all missions is collected for side-by-side comparison in table S1 in the Supplementary Materials. Although ecological ground truth for hotspot distributions was difficult to obtain in this real-world environment, we used the large carbonate skeleton of a dead *Dendrogyra cylindrus* pillar coral on the

northeast side of Joel's Shoal as a prominent landmark for a hotspot. On the basis of previous diver surveys, this coral skeleton was believed to be a likely hotspot of fish activity even after the coral polyps had died out. The visual fish census provided the lowest-noise observations of hotspot density, $P(Z_{s,\text{vis}}|X)$, because the AUV directly observed and localized visible organisms. However, the trade-off for this precision was the relatively limited extent, X, of the survey, which was limited by the field of view of the downward-facing camera.

We used an automated image processing pipeline to count the number of fish observed at each point along the survey trajectory (Fig. 4). The video showing the detection bounding boxes is included in the Supplementary Materials as movie S1. On average, we detected 1.86 fish per frame. However, these fish were not distributed uniformly. Fish were detected in only 3630 of 10,026 (36.2%) of frames, with 1597 (15.9%) containing multiple fish. When fish were present, an average of 5.14 fish were in frame, with a maximum of 65 fish detected in a single frame. This spatial heterogeneity matched a preliminary diver exploration of Joel's Shoal, which had identified three potential hotspot locations: the large *Dendrogyra* pillar coral pictured in Fig. 3 and two coral overhangs. These sites are shown with yellow, orange, and red circles, respectively, in Fig. 4. As can be seen in Fig. 4, the largest concentration of observed fish lies along the northeast edge of the reef near the *Dendrogyra* pillar coral. A second, less prominent hotspot was located ~5 m south of the first one. Using our fish census data, we were able to show an increase of 24.7 times the average number of fish per frame observed within 2 m of the *Dendrogyra* pillar coral and overhangs compared with the average across the rest of the survey. To validate these autonomously collected data, we manually counted fish in uniformly spaced 30-s intervals of diver survey videos taken during the same time span as our autonomous experiments. Manual survey data are shown in full in table S2. In the three frames where the *Dendrogyra* hotspot appeared, we counted 284, 34, and 40 fish for an average of 119.33. In frames where the *Dendrogyra* pillar coral did not appear, this average dropped to 12.67 fish ($N = 36$, $\sigma = 11.88$), for an average increase of 9.42 times.

A second postsurvey analysis of the visual data stitched the survey imagery into a three-dimensional (3D) orthomosaic of the reef (Fig. 4), using Metashape photogrammetry software (*64*). Using this mesh, we were able to quantify the rugosity of the reef (*65*), which has been shown to have a strong correlation with increased fish abundance and diversity in Caribbean reefs (*66*). In the survey area, we found that rugosity varied between 1.00 (flat ground in the sand flats on the eastern side of the reef) and 6.38 near the *Dendrogyra* pillar coral. Using a linear regression, we found that high-rugosity regions were correlated with the areas where the most fish were observed [regression slope (β) = 5.587 and coefficient of determination (R^2) = 0.34].

Acoustic hotspot mapping

The second experiment was a survey that constructed an acoustic map of fish density by triangulating fish calls using a directional hydrophone array. We conducted two of these passive acoustic surveys at Joel's Shoal. The first was during the same grid survey in November 2022 when the visual fish census data were collected. The second took place 8 months later in July 2023 and greatly expanded the survey area into a large cross-shaped survey with arms that extend 50 m north, south, east, and west from the center of Joel's Shoal reef. The *Dendrogyra* grid survey consisted of 57 observations each lasting 15 s and spaced every 2 m along the AUV's trajectory. During each of these observation windows, the AUV paused and drifted to avoid masking the reef soundscape with thruster noise. For the cross-survey, we made 44 observations, and the spacing between them was increased to 4.5 m. During the *Dendrogyra* grid survey, we detected 47 fish calls with confidence ≥0.4, for a call rate of 3.30 calls per minute, whereas the cross-survey had 66 detections and a call rate of 4.47 calls per minute. Heatmaps (Fig. 5) show the number of intersections between bearing vectors for detected fish calls over the reef. Given the time between observations and relatively short observation windows, it is highly unlikely that CUREE reobserved the same organism at multiple points during the survey. Even if it did, there would have been enough time between observations for the fish to have moved. However, past studies using PAM data have shown that the typical period of variability of fish on the reef is aligned with the daily cycle, with the most rapid changes happening at dawn and dusk (*23*, *67*). Given that we conducted our surveys near midday, we believe that the distribution of fish was stationary during the period of the survey. The acoustic surveys complemented the visual fish census data by directly addressing its limited extent, as demonstrated by the much larger cross-survey. However, this came at the cost of a noisier $P(Z_{s,\text{aud}}|X)$ because the AUV must infer organisms' positions rather than directly observe them.

As with the visual census shown in Fig. 4, the majority of the acoustic activity in both acoustic surveys was found on the northeast side of the reef, clustered around the high-rugosity areas near the *Dendrogyra* pillar coral and the two overhangs. Despite the 8 months between these two surveys, the position of this hotspot on the northeast side of Joel's Shoal remained consistent across the two acoustic surveys and was consistent with the hotspot identified by the visual census. However, the observed difference in the heatmap density between portions of the reef within 2 m of the *Dendrogyra* pillar coral and overhangs was substantially lower than in the visual census, only 1.8 times higher density on the *Dendrogyra* survey and 2.67 times during the cross-survey.

Acoustic homing using biological signatures

Although the open-loop visual and acoustic hotspot mapping experiments were successfully able to locate biological hotspots, they required considerable prior knowledge about the probable hotspot location to perform effectively. To discover hotspot environments where this assumption does not hold, such as exploring an previously unidentified reef, we developed a closed-loop acoustic homing behavior, which used CUREE's directional hydrophone array to guide the AUV to areas with substantial snapping shrimp activity (5 to 20 kHz). Figure 6 shows the results of two different sets of experiments conducted in March 2024 demonstrating this homing behavior. The first used an underwater speaker playing a recording of a healthy reef soundscape with shrimp snaps and fish vocalizations, which acted as a sound source with a known ground-truth position. We performed seven homing tracks using the speaker, during which the robot navigated toward the speaker from starting positions between 10 and 80 m away from the speaker at a variety of angles. CUREE was able to successfully navigate to the speaker each time, with an average final positional error of 3.891 m (SE = 0.809 m). During the longest track, the 80-m experiment shown in orange, a motor boat crossed the bay, necessitating a pause while the boat passed, which can be seen in the track 50 m away from the speaker at the 600-s mark.

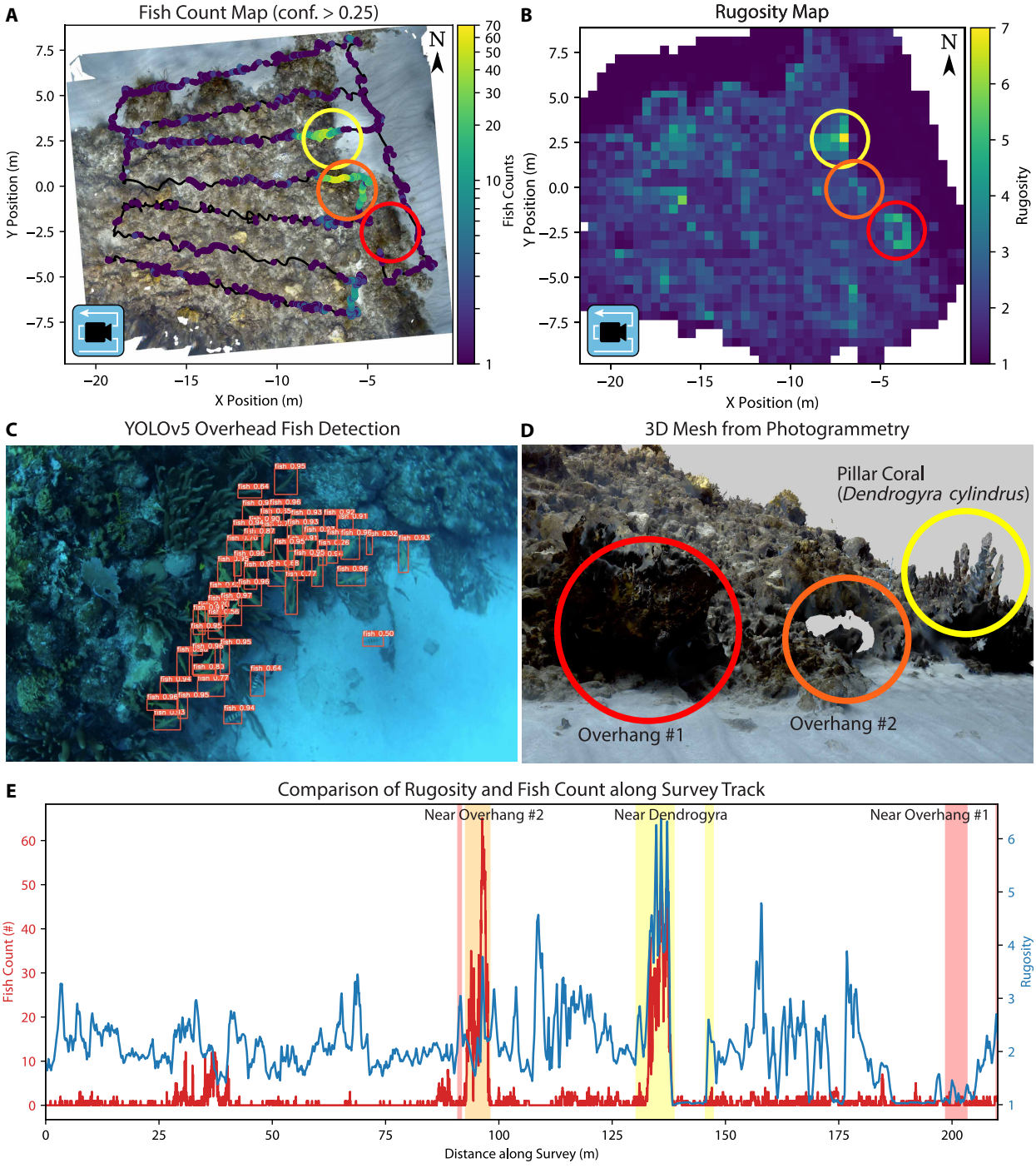

Fig. 4. Visual fish census of Joel's Shoal. (**A**) Map of visually detected fish during a lawnmower survey of Joel's Shoal and (**B**) map of rugosity of benthic substrate. (**C**) Individual fish were detected and counted using YOLOv5 (*83*). (**D**) High-rugosity areas included the *D. cylindrus* pillar coral and two overhangs highlighted with yellow, orange, and red circles, respectively. (**E**) Within 2 m of these high-rugosity features, the average number of fish per frame was 13.56, whereas the average across the rest of the reef was 0.55 fish per frame.

The second experiment was performed at Joel's Shoal using the natural soundscape of the reef as the acoustic source. For these experiments, we deployed the robot to the northeast of the reef, between 20 and 25 m from the reef, in a flat, sandy region. In both of the homing tracks, shown in Fig. 6, the emergent behavior can be seen as both trajectories converged on the large *Dendrogyra* pillar coral located on the northeast side of Joel's Shoal. Each trajectory passed close to the *Dendrogyra* pillar coral, with the closest point for the first trajectory 0.416 m away and the second 0.381 m. Once on the reef, the trajectories then took similar paths toward the reef center, where another, albeit much smaller, *Dendrogyra* colony was located. The first homing mission ran for 9 min 46 s, taking only 1 min

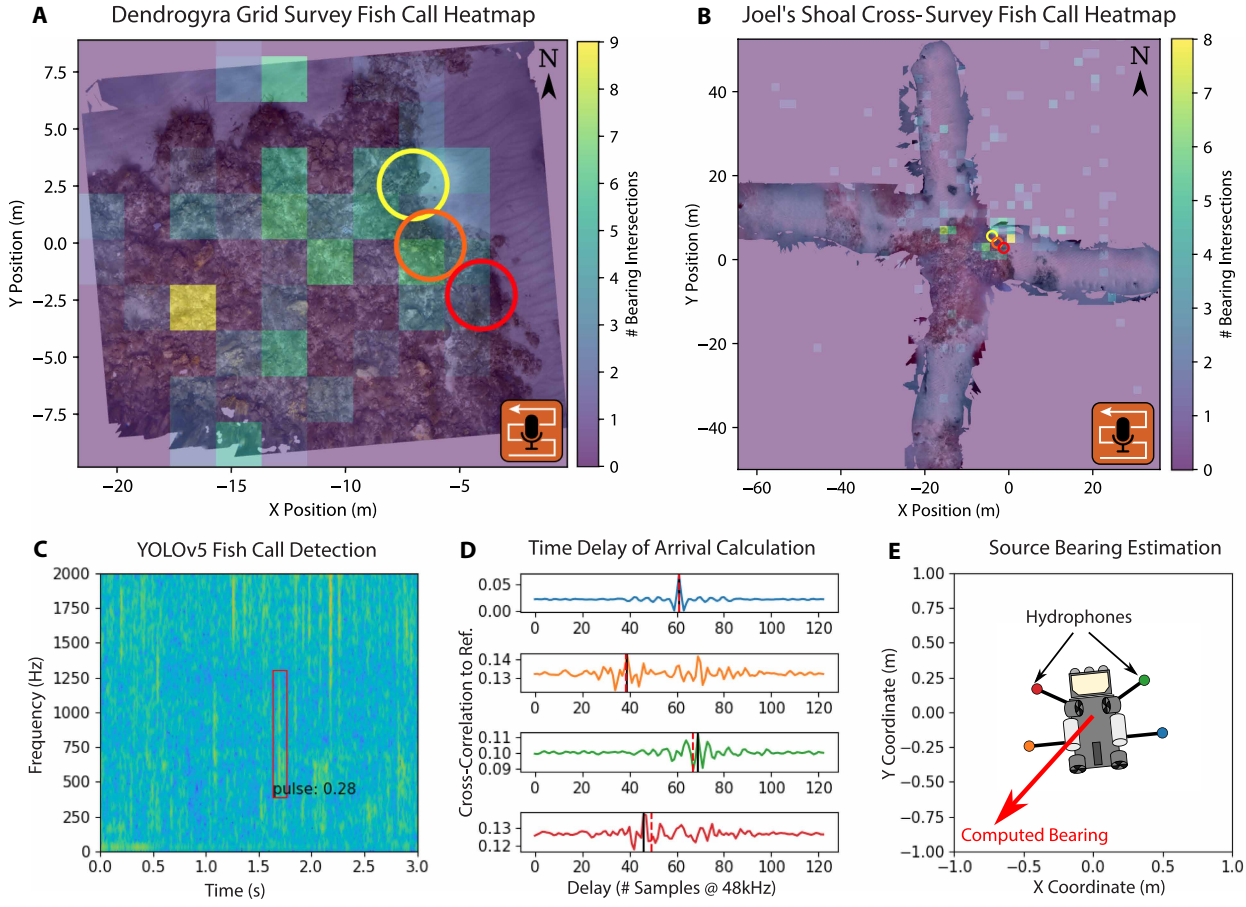

Fig. 5. Acoustic activity heatmaps for two surveys at Joel's Shoal. Heatmaps show the number of intersections of fish call detections (confidence ≥0.4) plotted at 2-m resolution. (**A**) A small-scale dense survey (*Dendrogyra* grid) and (**B**) a large-scale sparse survey (Joel's Shoal cross-survey). Both missions identified a primary acoustic hotspot near the *Dendrogyra* pillar coral on Joel's Shoal. Additional secondary hotspots near the center of the reef were also found in both surveys. The same *Dendrogyra* pillar coral and overhang locations from Fig. 3 are highlighted in the survey heatmaps. Heatmaps were produced by (**C**) detecting fish calls using a YOLO-based fish call detector (*24*), (**D**) computing TDOA using maximum cross-entropy, and (**E**) counting intersections between resultant bearing vectors.

32 s to arrive on the reef. The second mission started farther away and lasted 12 min 4 s, of which the first 3 min 46 s was the robot homing to the reef. Acoustic homing had the greatest hotspot discovery extent, *X*, of all four behaviors presented because it was not limited by a predefined survey area while also leveraging long-range acoustic sensing. However, its directness suffered even more than the acoustic survey, given that localizing an acoustic source while moving directly toward it requires arriving at the source location.

Visual tracking of sentinel species

Using vision-based gradient-following for hotspot discovery is challenging underwater because of the relatively low visibility compared with that in air (*68*). Instead, our fourth behavior addressed this range limitation by visually tracking an intermediary organism. We chose to use a sentinel species for this because these species are typically highly mobile, are visually distinct, and play critical ecological roles. For example, as a predator moves through its environment, it will bias its motion toward hotspots as it searches for patchily distributed resources. Over a sufficiently long duration, it will return repeatedly to hotspots where there is a high probability of finding prey (*69*, *70*), revealing their location.

In our experiment, we manually located a barracuda (*Sphyraena barracuda*), an apex predator on coral reefs. Using a semisupervised visual tracker, CUREE followed the barracuda for 9 min 55 s, over which time the AUV and barracuda moved a distance of 296 m over Joel's Shoal and surrounding regions. The barracuda was initially located near the *Dendrogyra* hotspot (Fig. 3). The path of the AUV is shown in Fig. 7. The full tracking sequence is included in the Supplementary Materials as movie S2. During the tracking mission, the AUV's behavior was predominantly autonomous, using visual servoing to keep the fish centered in the AUV's view. After the initial manual lock-on, the tracker required human intervention on seven occasions, either because the barracuda swam out of frame (a physical failure of the vehicle) or because the tracker had locked onto the wrong object (a failure of the tracking software). In total, these manual interventions accounted for 56 s of the track, with the remaining 8 min 59 s being fully autonomous.

Examining the trajectory of CUREE and the barracuda, we saw that the pair initially moved west, across Joel's Shoal, before going south then southeast, away from Joel's Shoal across a rocky region, and then along the edge of another previously unexplored reef. The barracuda then crossed a sandy region, heading west back toward

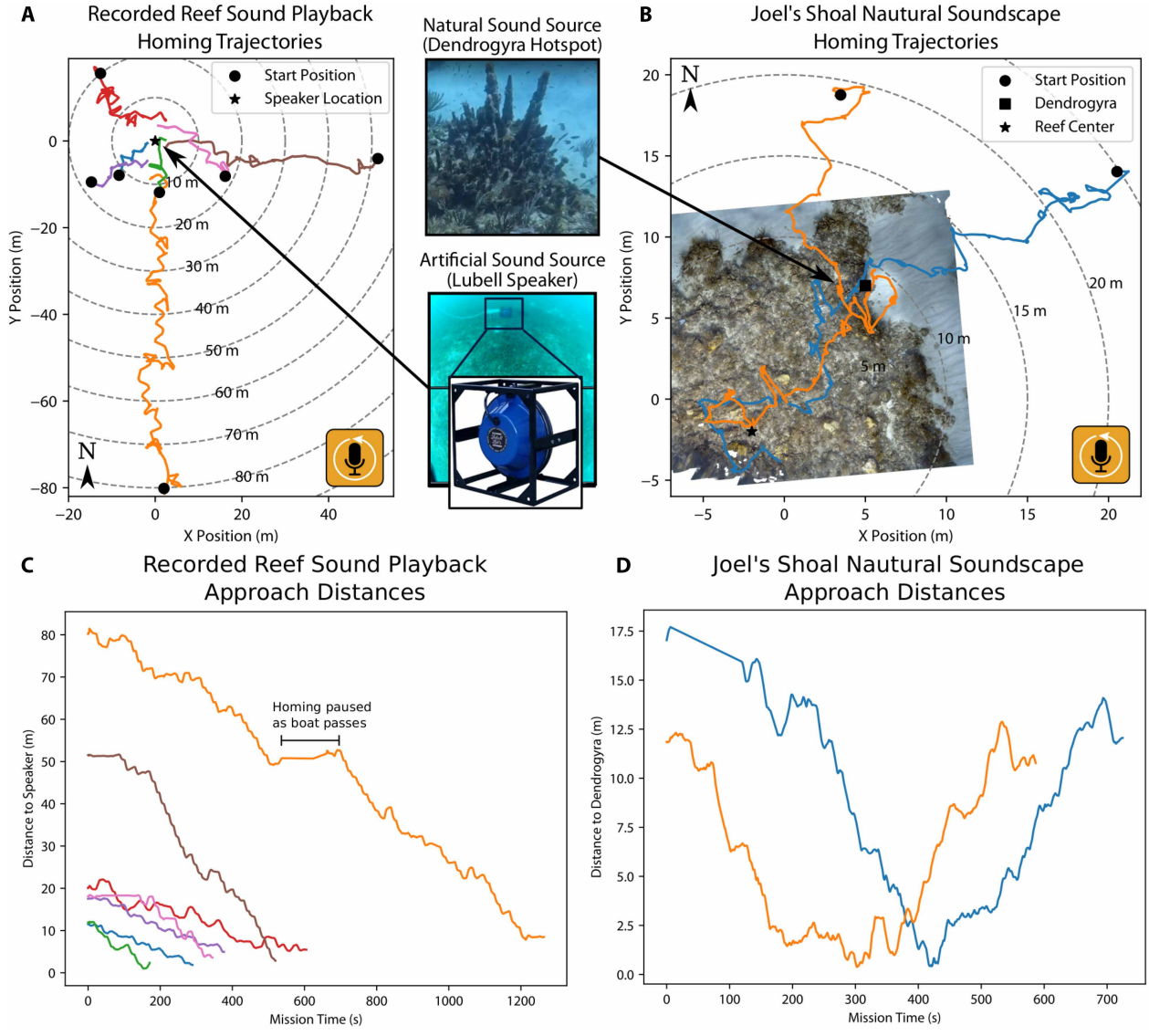

Fig. 6. Demonstration of passive acoustic homing with prerecorded reef sound playback and live reef sound at Joel's Shoal. (**A**) Trajectories from the recorded reef sound playback experiment show that CUREE was able to seek out the sound source at ranges of more than 80 m. (**B**) In the natural soundscape experiment at Joel's Shoal, CUREE's behavior was again consistent across both trajectories. Starting from two different points over sand to the northeast of the reef, CUREE homed in on acoustic signatures produced by biological activity near the *Dendrogyra* pillar coral and then proceeded southwest toward another acoustic hotspot. Approach distances to these hotspot locations are shown in (**C**) and (**D**), respectively.

Joel's Shoal and the *Dendrogyra* pillar coral. During the period when the barracuda was tracked, there were two points that the barracuda revisited. The first of these spots was the *Dendrogyra* hotspot identified in all of our previous experiments. The second was a spot roughly 50 m southeast of Joel's Shoal over a large sandy patch, where the barracuda revisited a point where it interacted with and scared off a large reef snapper. Although visual tracking offered the ability to discover unknown hotspots using purely short-ranged visual observations, it had relatively low directness, given that it relied on an assumption of ergodicity of the tracked organism relative to the hotspots.

DISCUSSION

The key result from our experiments was that each of the four hotspot discovery behaviors successfully and independently identified the northeast side of Joel's Shoal around the *Dendrogyra* pillar coral as the most biologically active portion of the reef. Furthermore, this hotspot was persistent across the experiments that spanned 15 months, pointing to this region as being consistently important as a home for a major portion of the biological activity of Joel's Shoal. The four hotspot discovery behaviors can be categorized by their type, either open-loop mapping or closed loop seeking, or by their sensing modality, either visual or acoustic. Each type and modality has advantages and disadvantages for discovering biological hotspots, which we discuss in more detail.

Multimodal sensing

Our experiments highlight the complementary nature of acoustic and visual sensing for discovering biological hotspots. During the *Dendrogyra* survey, the difference in the sharpness of the hotspot

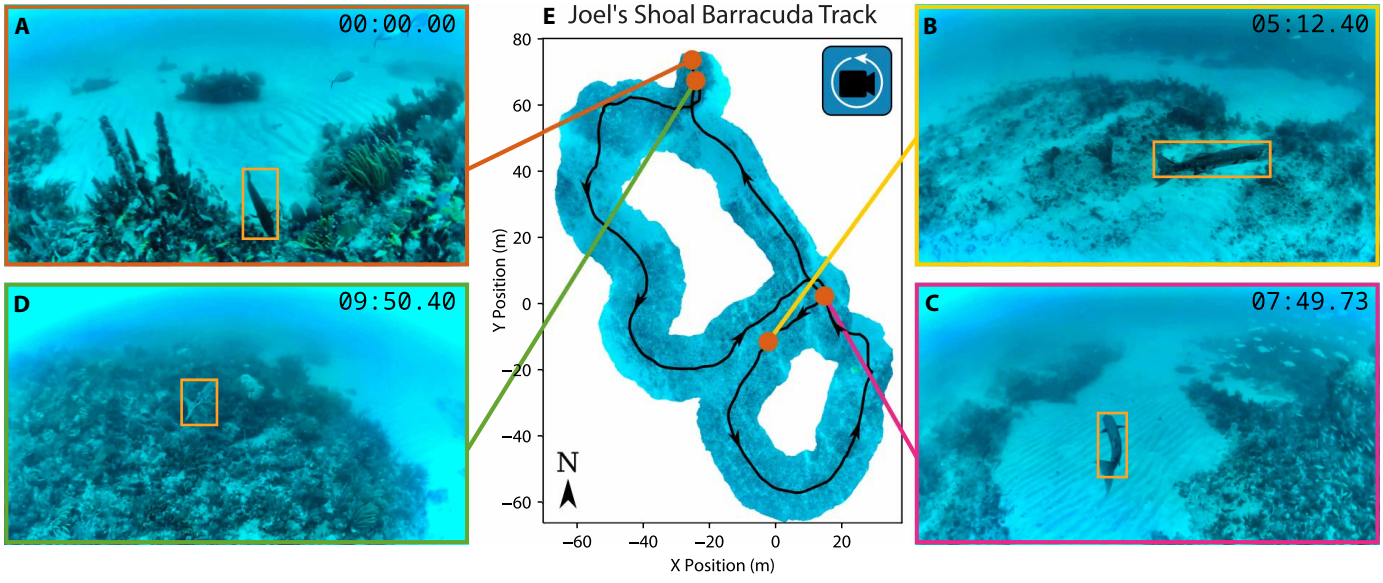

Fig. 7. Closed-loop visual tracking of a barracuda near Joel's Shoal. (**A**) The barracuda was first spotted near the Joel's Shoal *Dendrogyra* hotspot. The semisupervised tracker enabled the AUV to keep the fish in frame despite substantial appearance changes shown in profile view (**B**) or seen from behind (**C**) and (**D**). In these frames, the target of the tracker is shown in orange. (**E**) During the visual tracking experiment, CUREE followed a barracuda over a path length of 296 m as the fish traveled between two different reefs.

between the visual and acoustic maps highlights the difference in their respective directness. In the visual data, there is a sharp boundary of the hotspots with an increase of 24.7 times the number of fish observed within 2 m of the *Dendrogyra* pillar coral and overhangs compared with the average across the rest of the survey. In contrast, acoustic hotspot mapping produced much less prominent hotspots, only a 1.8-times increase. However, the trade-off for this loss of specificity is that, acoustically, we were able to replicate this result over much longer ranges, with the same hotspot being identified in the smaller *Dendrogyra* grid survey and the much larger Joel's Shoal cross-survey (Fig. 3). In the cross-survey, CUREE was able to detect fish calls located at this hotspot at ranges up to 25 m away. This distance is well beyond the range where the reef, let alone the fish on it, is visible to CUREE. Not only are these detection ranges aligned with existing literature (*34*, *45*), but they are also consistent between the acoustic mapping and acoustic homing experiments. In the demonstration of the homing behavior, the soundscape of Joel's Shoal was detected at ranges of up to 15 m from the reef.

Comparing the behavior of the active homing and tracking behaviors, the difference in directness follows from the selection of the respective choices of indicator species (Fig. 1): snapping shrimp for homing and the barracuda for tracking. The less-mobile snapping shrimp provide a more consistent signal toward the hotspot but offer less opportunity for discovery of multiple hotspots. These experiments also highlight another difference. During the visual track, because of the limited field of view of the camera, occasionally, the barracuda slipped out of frame, requiring a manual recovery to bring the barracuda back in frame. In contrast, acoustic homing uses an omnidirectional sensor, making it easier to reacquire the true biological signal and continue homing after the signal is temporarily masked, such as by the passing boat in Fig. 6.

By combining the two sensing modalities into a single mission, such as overlapping fish census and acoustic surveys, the limited-area visual data can be used to clarify the mapping between acoustic activity and abundance. This mapping can be used to predict species abundances across the regions of the map where only acoustic data are available. We used linear interpolation to compare gridded data (fish calls and rugosity) and point data (fish counts). Comparing the data collected in visual and acoustic surveys, we found a positive correlation between the number of visually observed fish and rugosity with $\beta = 4.352$ and $R^2 = 0.247$. We also found near-negligible correlations between rugosity and fish calls ($\beta = 0.457$ and $R^2 = 0.048$) and number of visually and acoustically observed fish ($\beta = 0.037$ and $R^2 = 0.024$). However, this dataset is dominated by frames with no visible fish or low numbers of fish (Fig. 4; 2993 of 10,026 total frames contained one or more fish, and only 973 frames contained three or more fish). This imbalance in the data makes it difficult for regression to pull out trends that only become apparent in the relatively rare hotspots where many fish are present. To account for this, we repeated the regression using only frames where at least one fish appeared. This resulted in a strengthening of the correlation between all three variables. Between rugosity and visual detections, we found $\beta = 6.587$ and $R^2 = 0.401$; between rugosity and fish calls, $\beta = 0.491$ and $R^2 = 0.101$; and between visual and acoustic detections, $\beta = 0.047$ and $R^2 = 0.099$. These regression data and additional filter values are shown in the Supplementary Materials (figs. S4 to S6). However, even filtering for only areas where fish are present does not fully explain the covariance between these variables. Other notable sources of variability may be the previously discussed difference in precision between the visual and acoustic modalities, visual observations of nonvocalizing fish species, or preferences by fish among high-rugosity regions. Other variables such as food availability can affect habitat preference and thus the formation of hotspots between areas of similar rugosity.

Open- and closed-loop control

Although all four hotspot discovery behaviors identified the northeast region of Joel's Shoal as a biological hotspot, they did so in different ways that affect the resultant distribution of observations,

$P(Z, X)$. The open-loop surveys were unguided, and, therefore, the expected time to locate an unknown point in space scales with the area (N^2) covered. In contrast, the guided search of the closed-loop methods scales with distance to the unknown point (N). This different scaling bears out in the mission times, where the grid survey and cross-survey at Joel's Shoal took 33 min 19 s and 44 min 55 s, respectively. In contrast, the two homing missions took nearly one-third of the time, only 12 min 5 s and 9 min 47 s, finding the *Dendrogyra* pillar coral in 7 min 0 s and 5 min 2 s, respectively. Although the barracuda track began at the *Dendrogyra* pillar coral, the barracuda quickly returned to the area, taking only 9 min 55 s to do so. The trade-off for this speed is completeness (*15*–*18*). Although the closed-loop missions found the hotspot more quickly and were equally capable at measuring the difference between the hotspot activity and surrounding baseline, they provided less context of the area around the hotspot and, therefore, were worse for mapping the spatial extent of the hotspot. Additionally, the systematic nature of the closed-loop behaviors had benefits for localization, providing loop closures to constrain visual localization and mapping algorithms (*13*, *71*) or to ensure overlapping features for 3D reconstruction (*72*).

In addition to a trade-off between speed and completeness when comparing open- versus closed-loop strategies, there are also interesting trade-offs when considering which sensing modality is used. The speedup in hotspot search is partially mitigated by the longer range offered using passive acoustics in a closed-loop behavior because triangulation for direct localization of the hotspot can be done with as few as two observations. However, acoustic localization accuracy is a function of the angular estimation error, which is location independent, and the ratio of the length of the triangulation baseline orthogonal to the (unknown) distance to the source. Dense coverage provides varied viewpoints, increasing both the length of the baseline and variability in the angle to the sound source. For both visual and acoustic sensing, repeated coverage of the same area in a single survey increases map accuracy. During visual mapping, multiple passes mitigate the multiple-detection problem that can arise when the robot sees the same fish or group of fish in multiple successive frames, whereas repeat visits with a passive acoustic sensor increase listening time and therefore the likelihood of observing a stochastic fish call.

For use in a multiyear data collection campaign, systematic mapping surveys offer replicability and direct comparisons of the same geographic region over time. Intuitively, because of their dense coverage of a predefined region of interest, both visual and acoustic mapping behaviors are particularly effective when there is a strong prior on the location of a hotspot and the objective is to quantify its magnitude and extent. In contrast, the two seeking behaviors, acoustic homing and visual tracking, provide more information when there is no such strong prior. Although we largely demonstrated each behavior in isolation, they can be combined as building blocks, enabling more complex and scientifically useful behaviors. By closing the control loop and leveraging data from the environment in real time, seeking behaviors allow an AUV to quickly converge on hotspot locations, collecting data that could be used to inform the placement of systematic grids for future mapping missions (*73*, *74*). This would allow the AUV to first seek out a hotspot over long ranges and, then, once found, precisely quantify each hotspots' size and biodiversity. The ultimate goal for our system is to become a scalable platform for assessing biodiversity across all types of ecosystems that can be placed in the hands of users around the globe.

Integration with ecological studies

Our system expands both the scale and scope of researchers' ability to study the distribution of biological hotspots on coral reefs. This represents a step forward in the ecological study of coral reefs, allowing biologists to pinpoint biological activity more quickly and with far higher spatial resolution than is now possible. Critically, our system can be integrated into existing experimental methodologies, using open-loop mapping behaviors to replicate pelagic diver surveys (*59*) and benthic photoquadrats (*75*). However, the principal contribution of our system lies in the AUV's ability to find and resolve hotspots within the boundaries of a reef. Traditional manual surveys of reefs are designed to assess the reef as a whole, averaging observations across a survey track (and multiple survey tracks) (*58*, *76*, *77*). Although this supports comparisons between reefs, it overlooks the hotspots and heterogeneity that occur within a reef but that are emerging as key components of ecosystem function and resilience (*58*, *78*, *79*). The 2D maps produced by our open-loop behaviors (Figs. 3 and 5) provide a more reliable and replicable way to study hotspot distributions on reefs than landmark-based annotation of diver video, such as in the manual comparison in the visual mapping experiment. Using these maps, we were able to directly quantify the importance of an area long suspected of being a hotspot. As stakeholders seek to prioritize areas of protection and how best to restore reefs, these quantitative assessments are vital.

Multimodal sensing also expands the scope of organisms that can be mapped using open and closed-loop behaviors. Some organisms that play an important role on the reef, such as urchins (*Diadema antillarum*), snapping shrimp (genera *Alpheus* and *Synalpheus*), and spiny lobsters (*Panulirus argus*), are cryptic and thus are difficult to observe visually. However, they are soniferous and thus available for acoustic detection and quantification. As demonstrated in acoustic homing, snapping shrimp provided a key resource for the AUV homing behavior. Similarly, simultaneous audio and visual hotspot mapping expands the scope of organisms that can be mapped to include soniferous cryptic organisms, allowing them to be included in larger-scale studies of reef health. Last, the simultaneous audio and visual observations directly address a long-standing limitation of PAM studies of coral reefs, namely, the inability of PAM sensing to effectively distinguish between different species. By collecting colocated audio and visual observations, we can begin to build datasets correlating the two sensing modalities, bridging this knowledge gap.

Through the inclusion of closed-loop behaviors and multimodal sensing, our system goes beyond what standard diver-based methods are capable of, enabling more targeted and higher-resolution studies of coral reef ecology. Acoustic homing enables active seeking of biological hotspots, which will facilitate the discovery of new active sites on unexplored coral reefs. Similarly, following individual organisms with visual tracking will allow scientists to obtain valuable information about the linkages among hotspots, animal behaviors, and habitats. The ability to quickly find and study new sites is particularly important in the face of myriad disturbances to coral reef ecosystems from natural and anthropogenic threats that can cause sweeping changes to coral reefs (*80*). Efficient and rapid discovery of now active sites can enable more targeted study and protection of more resilient portions of the reef. While tracking the barracuda, we found that it ventured into areas that were not previously considered to be part of the same reef system. Most surveys in the area, or similar studies, tend to focus surveys on the reef, where researchers and managers expect the highest concentration of life and tend to prioritize

management or studies. Last, long-term observations of a single organism provide opportunities to observe animal-animal interactions, such as the barracuda's territorial interaction with a large snapper. In doing so, we gain important data about the territorial interactions between these two predator species.

MATERIALS AND METHODS

Curious Underwater Robot for Ecosystem Exploration

The experiments shown here were conducted using CUREE (*60*), shown in Fig. 2. CUREE is a small single-person deployable AUV with six thrusters, enabling full six-degree-of-freedom motion underwater. For navigation, CUREE has a Water Linked A50 Doppler velocity logger (DVL) that measures speed over bottom and distance from the seafloor. It also has either a VectorNav VN-100 or ICM-20602 inertial measurement unit to measure orientation and acceleration, and it can be equipped with an Evologics S2C R 18/34 ultrashort baseline (USBL) system for absolute positioning underwater and transmitting basic commands and telemetry. CUREE used onboard batteries that provided 1.5 hours of operational duration. It carried all of the computation required for autonomous operations onboard, meaning that it could operate in either a tetherless or tethered configuration. While tethered, CUREE could be remotely controlled from a surface station, which also displayed real-time sensor data, including vehicle telemetry and high-resolution video. Although all of the experiments presented here except the Joel's Shoal cross-survey (Fig. 5) were conducted in the tethered configuration, all real-time data processing and control were performed on board CUREE. Across all experiments, CUREE operated at a nominal altitude of 2 m off the seafloor.

Visual sensing

CUREE's camera system is modular, but the typical configuration for our experiments consisted of two stereo camera pairs, one downward-facing and one forward-facing, each using Luxonis OAK-FFC-3P series boards combined with Arducam UC-517 Autofocus IMX477 modules and lenses with 110° fields of view. The angle of the forward-facing pair is configurable and can be varied between facing forward (90°) and facing downward at 60° or 45°. Modifying this camera configuration was done by swapping out the AUV's forward "head" housing (shown in Fig. 2), enabling CUREE to be quickly reconfigured for different mapping or tracking missions (*60*). Real-time data processing for the camera systems was also contained within the head, with an Nvidia Jetson Orin NX using a ConnectTech carrier board. The frame rate and resolution of these cameras were software configurable. The forward camera pair ran at 720p with 15 frames per second (fps) for fast closed-loop control for tracking and teleoperation (when tethered), and the downward pair was set to 1080p at 6 fps for high-resolution benthic mapping and 3D reconstruction.

Acoustic sensing

CUREE's passive acoustic sensors consisted of four calibrated HTI 96-MIN hydrophones with a sensitivity of −206 dB re: 1 V/μPa arranged in a planar array with a maximum aperture size of 0.88 m. Hydrophone data were gathered using an AcBotics AcSense DAQ with a 48-kHz sampling rate, which allowed CUREE to resolve sounds of up to 24 kHz. In the experiments shown here, we targeted the "fish band" (50 Hz to 2 kHz) and the "shrimp band" (4 to 20 kHz). We assumed that the overwhelming majority of acoustic sources were in the far field, far enough away from the robot that a wave propagating across the array will appear planar (*81*). The natural soundscape of the reef was 100.75 dB re: 1 $\mu Pa^2\ Hz^{-1}$, and individual fish calls had a signal-to-noise ratio of 1.53 (1.84 dB) over the noise floor (*24*, *58*). To avoid masking these sounds with the AUV's much louder thrusters, we adopted a listen-then-move strategy. When listening, CUREE would come to a stop then turn off its thrusters for a predefined amount of time. During the open-loop acoustic surveys, this was a 15-s window; however, during acoustic homing, this window duration was reduced to 3 s. When its thrusters were off, CUREE was not stationary. Because it was ballasted to be slightly positively buoyant, CUREE would slowly drift toward the surface when it was not actively maintaining depth. Additionally, CUREE was often subject to wave action and currents. For each recording, the first 1 s of data (0.5 s for homing) was discarded to ensure that no extraneous thruster spool-down noise would contaminate the reef soundscape recording. One other potential source of acoustic interference was the active acoustics, such as the DVL and USBL that CUREE used for state estimation. During the acoustic missions, the 23-kHz USBL, which would have interfered with biological signals, was not used, and we did not observe any acoustic leakage from the 1-MHz DVL into either the fish band or shrimp band.

Visual data processing

To count fish during the visual fish census, we used a semiautomated pipeline built around a YOLOv5 detector model (*82*, *83*). Our fish census imagery contained overhead views of fish and therefore was visually distinct from typical datasets of fish, which tend to focus on side profile views of fish or even fish out of water, such as in images of anglers holding fish. To account for this, we first trained the detector on a general corpus of annotated fish imagery from publicly available datasets: OzFish (*84*), FathomNet (only the Gnathostomata class) (*85*), FishTrack22 (*86*), Puget Sound Nearshore Fish (*87*), Labeled Fishes in the Wild (*88*), and DeepFish (segmentation only) (*89*). We followed this by fine-tuning the detector using manually annotated fish detections from 312 labeled frames out of a total of 13,236 recorded (2.3%) spaced evenly across our survey of Joel's Shoal. Last, we used this model to estimate fish counts on the remaining unlabeled images from the fish survey using a confidence threshold of 0.25. Where counts were available from hand-labeled data, those were used instead.

We computed rugosity, the ratio between actual surface area of an object and the portion of the 2D plane the object covers (*65*, *90*), using Metashape v2.1.2 (*64*) photogrammetry to produce 3D reconstructions of the reef and seafloor. Scale information was derived from CUREE's inertial odometry and AprilTags of known size in the resultant reconstructions, some of which can be seen in Fig. 4. Using the photogrammetry reconstruction, rugosity was computed at a 0.25-m^2 resolution.

For the visual tracking experiments, we used semisupervised tracking following the methodology outlined in (*91*), with KeepTrackFast (*92*) running onboard CUREE. This method used pretrained deep neural networks that compared reference images with patches in subsequent frames, localizing each subsequent patch most similar to the reference. In this way, only a single manually provided reference image was needed to provide robust tracking without the need for a comprehensive labeled dataset. This tracker was then integrated into the control stack of the vehicle in a simple visual-servoing scheme, where the tracked bounding box was maintained in the center of the vehicle's view. For the tracking mission, the vehicle was tethered,

allowing the operator to provide the initial bounding box using a graphical interface on the AUV's control station laptop and to intervene manually if the tracker lost its target. The tracker used the forward-facing cameras with an altitude safety threshold of 2 m.

Acoustic data processing

To map biological hotspots acoustically, we began by computing spectrograms from the recorded signals, and, then, using a YOLO-based fish call detector (*24*), we separated fish calls from the background soundscape. We retained each fish call with a predicted confidence threshold ≥0.4. For each call identified this way, we isolated it with a fourth-order Butterworth band-pass filter set by the upper and lower frequency bounds of the detected call. This filtered signal became the reference signal. Applying the same filter to each other channel, we computed the delay that maximized the cross-correlation with the reference signal. The final preprocessing step was to discard any bearings where the measured delays were physically implausible, for example, when a signal appeared to arrive at two opposite corners of the array in sequence before arriving at any other array elements. Assuming a known sound velocity c and distance between receivers, ΔD, the resultant delays can be used to compute the source angle θ with $\theta = \Delta D \times \frac{\cos^{-1}(\Delta t)}{c}$. With a planar array, CUREE could not disambiguate between sound sources arriving from above and below the robot. Given that most fish and invertebrate activity was observed near the reef bottom, we could reasonably assume the sounds came from below. However, this assumption was not necessary; because both mapping and homing behaviors were performed in 2D, we simply projected the resultant angles back into a 2D representation, flattening the Z axis and sidestepping the need to resolve this ambiguity entirely. The heatmaps shown in Fig. 5 are histograms showing the density of intersections between the rays for each detected fish call at each observation location, with bearing determined using time difference of arrival (TDOA) (*81*).

The relative infrequency of fish calls would have made them an unreliable signal for the short listening durations of the homing behavior. Instead, we used the more continuous noise of shrimp snapping (5 to 20 kHz) as the guide signal. However, the continuous signal prevented the use of TDOA to determine bearing. Thus, instead we used a real-time Bartlett beamformer (*93*), which subdivided the continuous acoustic signal into short windows, and used match filtering to determine a steering vector $\mathbf{a} = (\theta, \phi)$ where θ and ϕ are azimuth and elevation angles, respectively. The beamformer found an $\mathbf{a}$ that maximized $\mathbf{a}^H \times \mathbf{R} \times \mathbf{a}$, where H is the Hermitian operator and $\mathbf{R}$ is the covariance of time-averaged power of the signal (*81*). Given that snapping shrimp produce short, impulsive signals, we chose 0.1 s as the window size for the real-time beamformer (*93*). One issue that we encountered was that our array's aperture (0.88 m) was optimized for a narrowband frequency of 660 Hz and, because of signal aliasing, would create large side lobes at other frequencies. To address this, rather than using a single narrowband beamformer, we used a broadband beamformer created by averaging the output of 256 beamformers at uniformly spaced frequencies across the shrimp band. This averaging sufficiently damped the side lobes in the array response, obtaining a single narrow main lobe. We fitted a von Mises mixture to the distribution of bearings produced by the beamformer, and, then, we selected the mean of the highest-weighted component as the target bearing. During homing, CUREE would move 3 m along the target bearing, before it would come to a stop and repeat the process. The synthetic sound source experiment was conducted with the speaker placed on seafloor at a depth of 3 m in Great Lameshur Bay (latitude 18.318194, longitude −64.723612). The conditions in the bay during the experiment were calm (Beaufort sea state 1), and it was located far away from known reefs. Previous experimentation in Great Lameshur Bay found the ambient noise level substantially quieter than Joel's Shoal at 94.4 dB, making it an ideal location to test acoustic propagation in a natural environment (*94*). During the homing experiments, CUREE was manually driven to a point away from the source, and, then, the homing behavior was enabled. On Joel's Shoal, we set a maximum duration of 10 min. In Lameshur Bay, we terminated each homing experiment when the speaker came into view of the robot's cameras.

Statistical analysis of multimodal data

To identify correlations across different observation types (visual fish counts, acoustic maps, and rugosity), we used linear regression to fit β and R^2 to the data. Given that the acoustic heatmaps and rugosity data were gridded but the visual fish counts were not, we used linear interpolation from the gridded data to compute an estimate at the nongridded points, which was then used in linear regression. Both the linear interpolation and linear regression were implemented using the SciPy library in Python.

Site selection and context

Discovered in 2016, Joel's Shoal is a healthy coral reef located ~300 m southeast of Cocoloba Cay and 350 m south of Cocoloba Point on the southern coast of St. John (latitude 18.313309, longitude −64.757340), in the US Virgin Islands, and protected within the boundary of the Virgin Islands National Park. The reef consists of a rocky coral-covered region ~20 m by 30 m in size, surrounded by sandy flats with sparse seagrass and rubbly, sparse coral areas (Fig. 3). The reef's offshore location also helps to acoustically isolate it, mitigating the effects of other sound sources, such as waves breaking on the shore. Given that its location is generally leeward from the prevailing trade winds, conditions around Joel's Shoal are relatively mild (Beaufort scale ≤3). In these mild conditions, the effects of wind are not correlated with sound pressure levels (*58*).

Joel's Shoal is one of the best examples of a biologically active reef in the region, with high coral cover (4.8% hard coral cover and 25.1% soft coral cover) and low prevalence of macroalgae (*59*), allowing it to play host to a large number of fish and invertebrates (*23*, *76*), with a particularly large abundance of grunts and damselfish, both of which are taxa known for their acoustic activity (*95*, *96*). Joel's Shoal is part of a long-term reef assessment in the area and thus has been regularly characterized by standard diver surveys since 2016 (*59*) and has been the site of extensive PAM experiments (*24*, *76*).

Supplementary Materials

The PDF file includes:

Supplementary Text
Tables S1 to S3
Figs. S1 to S6

Other Supplementary Material for this manuscript includes the following:

Movies S1 and S2
Data files S1 and S2
MDAR Reproducibility Checklist

REFERENCES AND NOTES

1. W. V. Reid, Biodiversity hotspots. *Trends Ecol. Evol.* **13**, 275–280 (1998).
2. R. A. Mittermeier, W. R. Turner, F. W. Larsen, T. M. Brooks, C. Gascon, "Global biodiversity conservation: The critical role of hotspots" in *Biodiversity Hotspots: Distribution and Protection of Conservation Priority Areas*, F. E. Zachos, J. C. Habel, Eds. (Springer, 2011), pp. 3–22.
3. K. Benoit-Bird, T. Patrick Welch, C. Waluk, J. Barth, I. Wangen, P. McGill, C. Okuda, G. Hollinger, M. Sato, S. McCammon, Equipping an underwater glider with a new echosounder to explore ocean ecosystems. *Limnol. Oceanogr. Methods* **16**, 734–749 (2018).
4. M. K. Nolan, C. J. Kim, O. Hoegh-Guldberg, M. Beger, The benefits of heterogeneity in spatial prioritisation within coral reef environments. *Biol. Conserv.* **258**, 109155 (2021).
5. T. McClanahan, Local heterogeneity of coral reef diversity and environmental stress provides opportunities for small-scale conservation. *Divers. Distrib.* **29**, 1324–1340 (2023).
6. M. Spalding, A. Grenfell, New estimates of global and regional coral reef areas. *Coral Reefs* **16**, 225–230 (1997).
7. M. J. Costello, A. Cheung, N. De Hauwere, Surface area and the seabed area, volume, depth, slope, and topographic variation for the world's seas, oceans, and countries. *Environ. Sci. Technol.* **44**, 8821–8828 (2010).
8. N. Knowlton, R. E. Brainard, R. Fisher, M. Moews, L. Plaisance, M. J. Caley, "Coral reef biodiversity" in *Life in the World's Oceans: Diversity Distribution and Abundance*, A. D. McIntyre, Ed. (Blackwell, 2010) pp. 65–74.
9. J. Cant, L. Bramanti, G. Tsounis, Á. Martínez Quintana, H. R. Lasker, P. J. Edmunds, The recovery of octocoral populations following periodic disturbance masks their vulnerability to persistent global change. *Coral Reefs* **43**, 333–345 (2024).
10. O. Hoegh-Guldberg, W. Skirving, S. G. Dove, B. L. Spady, A. Norrie, E. F. Geiger, G. Liu, J. L. De La Cour, D. P. Manzello, Coral reefs in peril in a record-breaking year. *Science* **382**, 1238–1240 (2023).
11. T. D. Eddy, V. W. Lam, G. Reygondeau, A. M. Cisneros-Montemayor, K. Greer, M. L. D. Palomares, J. F. Bruno, Y. Ota, W. W. Cheung, Global decline in capacity of coral reefs to provide ecosystem services. *One Earth* **4**, 1278–1285 (2021).
12. H. Singh, R. Armstrong, F. Gilbes, R. Eustice, C. Roman, O. Pizarro, J. Torres, Imaging coral I: Imaging coral habitats with the SeaBED AUV. *Subsurface Sens. Technol. Appl.* **5**, 25–42 (2004).
13. S. B. Williams, O. Pizarro, J. M. Webster, R. J. Beaman, I. Mahon, M. Johnson-Roberson, T. C. Bridge, Autonomous underwater vehicle–assisted surveying of drowned reefs on the shelf edge of the Great Barrier Reef, Australia. *J. Field Robot.* **27**, 675–697 (2010).
14. T. Jackson-Bué, G. J. Williams, G. Walker-Springett, S. J. Rowlands, A. J. Davies, Three-dimensional mapping reveals scale-dependent dynamics in biogenic reef habitat structure. *Remote Sens. Ecol. Conserv.* **7**, 621–637 (2021).
15. R. Wartenberg, A. Booth, Video transects are the most appropriate underwater visual census method for surveying high-latitude coral reef fishes in the southwestern Indian Ocean. *Mar. Biodivers.* **45**, 633–646 (2015).
16. A. R. Halford, A. A. Thompson, *Visual Census Surveys of Reef Fish* (Australian Institute of Marine Science, 1994).
17. M. Kulbicki, N. Cornuet, L. Vigliola, L. Wantiez, G. Moutham, P. Chabanet, Counting coral reef fishes: Interaction between fish life-history traits and transect design. *J. Exp. Mar. Biol. Ecol.* **387**, 15–23 (2010).
18. R. T. Hanlon, G. McManus, Flamboyant cuttlefish behavior: Camouflage tactics and com-plex colorful reproductive behavior assessed during field studies at Lembeh Strait, Indonesia. *J. Exp. Mar. Biol. Ecol.* **529**, 151397 (2020).
19. G. Courtenay, D. R. Smith, W. Gladstone, Occupational health issues in marine and freshwater research. *J. Occup. Med. Toxicol.* **7**, 4 (2012).
20. A. Heenan, I. D. Williams, T. Acoba, A. DesRochers, R. K. Kosaki, T. Kanemura, M. O. Nadon, R. E. Brainard, Long-term monitoring of coral reef fish assemblages in the western central Pacific. *Sci. Data* **4**, 170176 (2017).
21. P. Molloy, M. Evanson, A. Nellas, J. Rist, J. Marcus, H. Koldewey, A. Vincent, How much sampling does it take to detect trends in coral-reef habitat using photoquadrat surveys? *Aquat. Conserv.: Mar. Freshw. Ecosyst.* **23**, 820–837 (2013).
22. A. Lillis, F. Caruso, T. A. Mooney, J. Llopiz, D. Bohnenstiehl, D. B. Eggleston, Drifting hydrophones as an ecologically meaningful approach to underwater soundscape measurement in coastal benthic habitats. *J. Ecoacoustics* **2**, 10.22261/JEA.STBDH1 (2018).
23. S. D. Jarriel, N. Formel, S. R. Ferguson, F. H. Jensen, A. Apprill, T. A. Mooney, Unidentified fish sounds as indicators of coral reef health and comparison to other acoustic methods. *Front. Remote Sens.* **5**, 1338586 (2024).
24. S. McCammon, N. Formel, S. Jarriel, T. A. Mooney, Rapid detection of fish calls within diverse coral reef soundscapes using a convolutional neural network. *J. Acoust. Soc. Am.* **157**, 1665–1683 (2025).
25. M. O. Lammers, L. M. Munger, "From shrimp to whales: Biological applications of passive acoustic monitoring on a remote Pacific coral reef" in *Listening in the Ocean*, W. W. L. Au, M. O. Lammers, Eds. (Springer, 2016), pp. 61–81.
26. T. C. Tricas, K. S. Boyle, Acoustic behaviors in Hawaiian coral reef fish communities. *Mar. Ecol. Prog. Ser.* **511**, 1–16 (2014).
27. A. Looby, C. Erbe, S. Bravo, K. Cox, H. L. Davies, L. Di Iorio, Y. Jézéquel, F. Juanes, C. W. Martin, T. A. Mooney, C. Radford, L. K. Reynolds, A. N. Rice, A. Riera, R. Rountree, B. Spriel, J. Stanley, S. Vela, M. J. G. Parsons, Global inventory of species categorized by known underwater sonifery. *Sci. Data* **10**, 892 (2023).
28. T. A. Mooney, L. Di Iorio, M. Lammers, T.-H. Lin, S. L. Nedelec, M. Parsons, C. Radford, E. Urban, J. Stanley, Listening forward: Approaching marine biodiversity assessments using acoustic methods. *R. Soc. Open Sci.* **7**, 201287 (2020).
29. D. A. Mann, P. S. Lobel, Acoustic behavior of the damselfish *Dascyllus albisella*: Behavioral and geographic variation. *Environ. Biol. Fishes* **51**, 421–428 (1998).
30. P. Lobel, I. Kaatz, A. Rice, "Acoustical behavior of coral reef fishes" in *Reproduction and Sexuality in Marine Fishes: Patterns and Processes*, K. S. Cole, Ed. (University of California Press, 2010), pp. 307–386.
31. T. C. Tricas, K. S. Boyle, Parrotfish soundscapes: Implications for coral reef management. *Mar. Ecol. Prog. Ser.* **666**, 149–169 (2021).
32. C. Radford, A. Jeffs, C. Tindle, J. C. Montgomery, Resonating sea urchin skeletons create coastal choruses. *Mar. Ecol. Prog. Ser.* **362**, 37–43 (2008).
33. S. E. Freeman, L. A. Freeman, G. Giorli, A. F. Haas, Photosynthesis by marine algae produces sound, contributing to the daytime soundscape on coral reefs. *PLOS ONE* **13**, e0201766 (2018).
34. D. A. Mann, P. S. Lobel, Propagation of damselfish (Pomacentridae) courtship sounds. *J. Acoust. Soc. Am.* **101**, 3783–3791 (1997).
35. J. A. Stanley, S. M. Van Parijs, L. T. Hatch, Underwater sound from vessel traffic reduces the effective communication range in Atlantic cod and haddock. *Sci. Rep.* **7**, 14633 (2017).
36. A. K. Salas, M. S. Ballard, T. A. Mooney, P. S. Wilson, Effects of frequency-dependent spatial variation in soundscape settlement cues for reef fish larvae. *Mar. Ecol. Prog. Ser.* **687**, 1–21 (2022).
37. S. P. González-Sabbagh, A. Robles-Kelly, A survey on underwater computer vision. *ACM Comput. Surv.* **55**, 1–39 (2023).
38. A. Filisetti, A. Marouchos, A. Martini, T. Martin, S. Collings, "Developments and applications of underwater LiDAR systems in support of marine science" in *OCEANS 2018 MTS/IEEE Charleston* (IEEE, 2018), pp. 1–10.
39. A. Salman, A. Jalal, F. Shafait, A. Mian, M. Shortis, J. Seager, E. Harvey, Fish species classification in unconstrained underwater environments based on deep learning. *Limnol. Oceanogr. Methods* **14**, 570–585 (2016).
40. K. M. Knausgard, A. Wiklund, T. K. Sørdalen, K. T. Halvorsen, A. R. Kleiven, L. Jiao, M. Goodwin, Temperate fish detection and classification: A deep learning based approach. *Appl. Intell.* **52**, 6988–7001 (2022).
41. A. Saleh, M. Sheaves, M. Rahimi Azghadi, Computer vision and deep learning for fish classification in underwater habitats: A survey. *Fish Fish.* **23**, 977–999 (2022).
42. X. Mouy, S. K. Archer, S. Dosso, S. Dudas, P. English, C. Foord, W. Halliday, F. Juanes, D. Lancaster, S. Van Parijs, D. Haggarty, Automatic detection of unidentified fish sounds: A comparison of traditional machine learning with deep learning. *Front. Remote Sens.* **5**, 1439995 (2024).
43. M. Picciulin, L. Kéver, E. Parmentier, M. Bolgan, Listening to the unseen: Passive acoustic monitoring reveals the presence of a cryptic fish species. *Aquat. Conserv.: Mar. Freshw. Ecosyst.* **29**, 202–210 (2019).
44. E. Parmentier, F. Bertucci, M. Bolgan, D. Lecchini, How many fish could be vocal? An estimation from a coral reef (Moorea Island). *Belg. J. Zool.* **151**, 10.26496/bjz.2021.82 (2021).
45. C. Lembke, S. Grasty, A. Silverman, H. Broadbent, S. Butcher, S. Murawski, The camera-based assessment survey system (C-BASS): A towed camera platform for reef fish abundance surveys and benthic habitat characterization in the Gulf of Mexico. *Cont. Shelf Res.* **151**, 62–71 (2017).
46. T. Davis, G. Cadiou, J. Williams, M. Coleman, Costs and benefits of towed videos and remotely operated vehicles for sampling shallow reef habitats and fish. *Mar. Freshw. Res.* **71**, 953–961 (2019).
47. S. McCammon, G. A. Hollinger, "Planning and executing optimal non-entangling paths for teth-ered underwater vehicles" in *2017 IEEE International Conference on Robotics and Automation (ICRA)* (IEEE, 2017), pp. 3040–3046.
48. A. K. Cresswell, N. M. Ryan, A. J. Heyward, A. N. Smith, J. Colquhoun, M. Case, M. J. Birt, M. Chinkin, M. Wyatt, B. Radford, P. Costello, J. P. Gilmour, A quantitative comparison of towed-camera and diver-camera transects for monitoring coral reefs. *PeerJ* **9**, e11090 (2021).
49. M. Massot-Campos, T. Yamada, B. Walker-Rouse, K. Collins, J. Leyland, H. Kassem, B. Thornton, "Shallow water seagrass survey at Studland Bay with the AUV Smarty200" in *2023 IEEE Underwater Technology (UT)* (IEEE, 2023), pp. 1–5.
50. S. Williams, I. Mahon, "Simultaneous localisation and mapping on the great barrier reef" in *IEEE International Conference on Robotics and Automation, 2004. Proceedings. ICRA'04. 2004* (IEEE, 2004), vol. 2, pp. 1771–1776.
51. G. Billings, R. Camilli, M. Johnson-Roberson, Hybrid visual SLAM for underwater vehicle manipulator systems. *IEEE Robot. Autom. Lett.* **7**, 6798–6805 (2022).

52. M. E. Clarke, C. Whitmire, E. Fruh, J. Anderson, J. Taylor, J. Rooney, S. Ferguson, H. Singh, "Developing the SeaBED AUV as a tool for conducting routine surveys of fish and their habitat in the Pacific" in *2010 IEEE/OES Autonomous Underwater Vehicles* (IEEE, 2010), pp. 1–5.
53. J. Z. Nash, J. Bond, M. Case, I. McCarthy, R. Mowat, I. Pierce, W. Teahan, Tracking the fine scale movements of fish using autonomous maritime robotics: A systematic state of the art review. *Ocean Eng.* **229**, 108650 (2021).
54. D. R. Yoerger, A. F. Govindarajan, J. C. Howland, J. K. Llopiz, P. H. Wiebe, M. Curran, J. Fujii, D. Gomez-Ibanez, K. Katija, B. H. Robison, B. W. Hobson, M. Risi, S. M. Rock, A hybrid underwater robot for multidisciplinary investigation of the ocean twilight zone. *Sci. Robot.* **6**, eabe1901 (2021).
55. K. Barnard, J. Daniels, P. L. Roberts, E. C. Orenstein, I. Masmitja, J. Takahashi, B. Woodward, K. Katija, DeepSTARia: Enabling autonomous, targeted observations of ocean life in the deep sea. *Front. Mar. Sci.* **11**, 1357879 (2024).
56. H. K. Meyer, E. M. Roberts, H. T. Rapp, A. J. Davies, Spatial patterns of arctic sponge ground fauna and demersal fish are detectable in autonomous underwater vehicle (AUV) imagery. *Deep Sea Res. I Oceanogr. Res. Pap.* **153**, 103137 (2019).
57. K. J. Morris, B. J. Bett, J. M. Durden, V. A. Huvenne, R. Milligan, D. O. Jones, S. McPhail, K. Robert, D. M. Bailey, H. A. Ruhl, A new method for ecological surveying of the abyss using autonomous underwater vehicle photography. *Limnol. Oceanogr. Methods* **12**, 795–809 (2014).
58. M. B. Kaplan, T. A. Mooney, J. Partan, A. R. Solow, Coral reef species assemblages are associated with ambient soundscapes. *Mar. Ecol. Prog. Ser.* **533**, 93–107 (2015).
59. C. C. Becker, L. Weber, J. K. Llopiz, T. A. Mooney, A. Apprill, Microorganisms uniquely capture and predict stony coral tissue loss disease and hurricane disturbance impacts on US Virgin Island reefs. *Environ. Microbiol.* **26**, e16610 (2024).
60. Y. Girdhar, N. McGuire, L. Cai, S. Jamieson, S. McCammon, B. Claus, J. E. San Soucie, J. E. Todd, T. A. Mooney, "CUREE: A curious underwater robot for ecosystem exploration" in *2023 IEEE International Conference on Robotics and Automation (ICRA)* (IEEE, 2023), pp. 11411–11417.
61. I. W. Renner, J. Elith, A. Baddeley, W. Fithian, T. Hastie, S. J. Phillips, G. Popovic, D. I. Warton, Point process models for presence-only analysis. *Methods Ecol. Evol.* **6**, 366–379 (2015).
62. S. Russell, P. Norvig, in *Artificial Intelligence: A Modern Approach* (Prentice-Hall, 1995).
63. E. Galceran, M. Carreras, A survey on coverage path planning for robotics. *Robot. Autonom. Syst.* **61**, 1258–1276 (2013).
64. Agisoft, Metashape, www.agisoft.com/downloads/installer/.
65. A. Friedman, O. Pizarro, S. B. Williams, M. Johnson-Roberson, Multi-scale measures of rugosity, slope and aspect from benthic stereo image reconstructions. *PLOS ONE* **7**, e50440 (2012).
66. B. Gratwicke, M. R. Speight, Effects of habitat complexity on Caribbean marine fish assemblages. *Mar. Ecol. Prog. Ser.* **292**, 301–310 (2005).
67. A. Lillis, A. Apprill, M. Armenteros, T. A. Mooney, "Small-scale variation in the soundscapes of coral reefs" in *The Effects of Noise on Aquatic Life: Principles and Practical Considerations*, A. N. Popper, J. Sisneros, A. D. Hawkins, F. Thomsen, Eds. (Springer, 2023), pp. 1–15.
68. S. Jamieson, J. P. How, Y. Girdhar, "DeepSeeColor: Realtime adaptive color correction for autonomous underwater vehicles via deep learning methods" in *2023 IEEE International Conference on Robotics and Automation (ICRA)* (IEEE, 2023), pp. 3095–3101.
69. O. Vilk, Y. Orchan, M. Charter, N. Ganot, S. Toledo, R. Nathan, M. Assaf, Ergodicity breaking in area-restricted search of avian predators. *Phys. Rev. X* **12**, 031005 (2022).
70. R. Nathan, C. T. Monk, R. Arlinghaus, T. Adam, J. Alós, M. Assaf, H. Baktoft, C. E. Beardsworth, M. G. Bertram, T. Bijleveld, A. I. Brodin, J. L. Brooks, A. Campos-Candela, S. J. Cooke, K. Ø. Gjelland, P. R. Gupte, R. Harel, G. Hellström, F. Jeltsch, S. S. Killen, T. Klefoth, R. Langrock, R. J. Lennox, E. Lourie, J. R. Madden, Y. Orchan, I. S. Pauwels, M. Říha, M. Roeleke, U. E. Schlägel, D. Shohami, J. Signer, S. Toledo, O. Vilk, S. Westrelin, M. A. Whiteside, I. Jarić, Big-data approaches lead to an increased understanding of the ecology of animal movement. *Science* **375**, eabg1780 (2022).
71. S. Hong, J. Kim, J. Pyo, S.-C. Yu, A robust loop-closure method for visual SLAM in unstructured seafloor environments. *Auton. Robot.* **40**, 1095–1109 (2016).
72. M. Johnson-Roberson, O. Pizarro, S. B. Williams, I. Mahon, Generation and visualization of large-scale three-dimensional reconstructions from underwater robotic surveys. *J. Field Robot.* **27**, 21–51 (2010).
73. S. Kemna, O. Kroemer, G. S. Sukhatme, "Pilot surveys for adaptive informative sampling" in *2018 IEEE International Conference on Robotics and Automation (ICRA)* (IEEE, 2018), pp. 6417–6424.
74. A. S. Ferreira, M. Costa, F. Py, J. Pinto, M. A. Silva, A. Nimmo-Smith, T. A. Johansen, J. B. de Sousa, K. Rajan, Advancing multi-vehicle deployments in oceanographic field experiments. *Auton. Robot.* **43**, 1555–1574 (2019).
75. P. J. Edmunds, Decadal-scale changes in the community structure of coral reefs of St. John, US Virgin Islands. *Mar. Ecol. Prog. Ser.* **489**, 107–123 (2013).
76. J. P. Dinh, J. J. Suca, A. Lillis, A. Apprill, J. K. Llopiz, T. A. Mooney, Multiscale spatio-temporal patterns of boat noise on US Virgin Island coral reefs. *Mar. Pollut. Bull.* **136**, 282–290 (2018).
77. N. P. Jones, R. R. Ruzicka, M. A. Colella, M. S. Pratchett, D. S. Gilliam, Frequent disturbances and chronic pressures constrain stony coral recovery on Florida's Coral Reef. *Coral Reefs* **41**, 1665–1679 (2022).
78. E. Staaterman, S. J. Brandl, M. Hauer, J. M. Casey, A. J. Gallagher, A. N. Rice, Individual voices in a cluttered soundscape: Acoustic ecology of the Bocon toadfish, *Amphichthys cryptocentrus*. *Environ. Biol. Fishes* **101**, 979–995 (2018).
79. S. E. Freeman, F. L. Rohwer, G. L. D'Spain, A. M. Friedlander, A. K. Gregg, S. A. Sandin, M. J. Buckingham, The origins of ambient biological sound from coral reef ecosystems in the Line Islands archipelago. *J. Acoust. Soc. Am.* **135**, 1775–1788 (2014).
80. T. P. Hughes, M. J. Rodrigues, D. R. Bellwood, D. Ceccarelli, O. Hoegh-Guldberg, L. McCook, N. Moltschaniwskyj, M. S. Pratchett, R. S. Steneck, B. Willis, Phase shifts, herbivory, and the resilience of coral reefs to climate change. *Curr. Biol.* **17**, 360–365 (2007).
81. D. H. Johnson, D. E. Dudgeon, *Array Signal Processing: Concepts and Techniques* (Prentice-Hall, 1992).
82. J. Redmon, S. Divvala, R. Girshick, A. Farhadi, "You only look once: Unified, real-time object detection" in *Proceedings of the IEEE Conference on Computer Vision and Pattern Recognition* (IEEE, 2016), pp. 779–788.
83. G. Jocher, A. Stoken, J. Borovec, L. Changyu, A. Hogan, L. Diaconu, J. Poznanski, L. Yu, P. Rai, R. Ferriday, T. Sullivan, W. Xinyu, E. R. Claramunt, P. Dave, ultralytics/yolov5: v3.0, Zenodo (2020); https://zenodo.org/records/3983579.
84. D. Marrable, K. Barker, S. Tippaya, M. Wyatt, S. Bainbridge, M. Stowar, J. Larke, Accelerating species recognition and labelling of fish from underwater video with machine-assisted deep learning. *Front. Mar. Sci.* **9**, 944582 (2022).
85. K. Katija, E. Orenstein, B. Schlining, L. Lundsten, K. Barnard, G. Sainz, O. Boulais, M. Cromwell, E. Butler, B. Woodward, K. L. C. Bell, FathomNet: A global image database for enabling artificial intelligence in the ocean. *Sci. Rep.* **12**, 15914 (2022).
86. M. Dawkins, M. Lucero, T. Banez, R. Faillettaz, M. Campbell, J. Prior, B. Richards, A. Rollo, A. Chaudhary, A. Hoogs, M. Salvi, B. Lewis, B. Davis, N. Siekierski, "FishTrack22: An ensemble dataset for automatic tracking evaluation," poster presented at CV4Animals: Computer Vision for Animal Behavior Tracking and Modeling (workshop), 20 June 2022, New Orleans, LA, USA.
87. B. Ferriss, K. Veggerby, M. Bogeberg, L. Conway-Cranos, L. Hoberecht, P. Kiffney, K. Litle, J. Toft, B. Sanderson, Characterizing the habitat function of bivalve aquaculture using underwater video. *Aquac. Environ. Interact.* **13**, 439–454 (2021).
88. G. Cutter, K. Stierhoff, J. Zeng, "Automated detection of rockfish in unconstrained underwater videos using Haar cascades and a new image dataset: Labeled fishes in the wild" in *2015 IEEE Winter Applications and Computer Vision Workshops* (IEEE, 2015), pp. 57–62.
89. A. Saleh, I. H. Laradji, D. A. Konovalov, M. Bradley, D. Vazquez, M. Sheaves, A realistic fish-habitat dataset to evaluate algorithms for underwater visual analysis. *Sci. Rep.* **10**, 14671 (2020).
90. M. J. Risk, "Fish diversity on a coral reef in the Virgin Islands," Atoll Research Bulletin no. 153 (Smithsonian Institution, 1972).
91. L. Cai, N. E. McGuire, R. Hanlon, T. A. Mooney, Y. Girdhar, Semi-supervised visual tracking of marine animals using autonomous underwater vehicles. *Int. J. Comput. Vis.* **131**, 1406–1427 (2023).
92. C. Mayer, M. Danelljan, D. P. Paudel, L. Van Gool, "Learning target candidate association to keep track of what not to track" in *Proceedings of the IEEE/CVF International Conference on Computer Vision* (IEEE, 2021), pp. 13444–13454.
93. S. McCammon, S. Jamieson, T. A. Mooney, Y. Girdhar, "Discovering biological hotspots with a passively listening AUV" in *2024 IEEE International Conference on Robotics and Automation (ICRA)* (IEEE, 2024), pp. 3789–3795.
94. Y. Jézéquel, N. Aoki, T. A. Mooney, Acoustic properties and shallow water propagation distances of Caribbean spiny lobster sounds (*Panulirus argus*). *J. Acoust. Soc. Am.* **153**, 529–537 (2023).
95. S. A. Egner, D. A. Mann, Auditory sensitivity of sergeant major damselfish *Abudefduf saxatilis* from post-settlement juvenile to adult. *Mar. Ecol. Prog. Ser.* **285**, 213–222 (2005).
96. F. Bertucci, L. Ruppé, S. Van Wassenbergh, P. Compère, E. Parmentier, New insights into the role of the pharyngeal jaw apparatus in the sound-producing mechanism of *Haemulon flavolineatum* (Haemulidae). *J. Exp. Biol.* **217**, 3862–3869 (2014).
97. W. L. Buntine, Operations for learning with graphical models. *J. Artif. Intell. Res.* **2**, 159–225 (1994).

Acknowledgments: We dedicate this paper to the memory of Joel Llopiz, the discoverer and namesake of our study site, Joel's Shoal. Without Joel's pioneering efforts studying reefs on St. John, the work presented here would not be possible. We also acknowledge the help of the WHOI Reef Solutions Initiative team. In particular, we recognize the specific contributions of S. Jamieson and N. McGuire for the assistance with the development of the CUREE platform, N. Formel and S. Jarriel for the assistance during the USVI field campaigns, S. Spintado-Verner

for analysis of diver survey data for Joel's Shoal, and F. Jensen for insights into passive acoustic data processing. Last, we recognize the University of the Virgin Islands and the Virgin Islands Environmental Resource Station for making our field work possible. **Funding:** This work was supported, in part, by NSF grant nos. 2133029 and 2024077, the Joint Initiative Awards Fund from the Andrew W. Mellon Foundation, and the Postdoctoral Scholar Program at Woods Hole Oceanographic Institution, with funding provided by the Doherty Foundation. The experiments were conducted under National Park Service Scientific Research and Collecting Permits VIIS-2022-SCI-0005. **Author contributions:** S.M. developed the passive acoustic hardware and software used for the acoustic mapping and homing methods and was the principal author of this manuscript. L.C. led the visual tracking work. L.C. and D.Y. developed the visual fish census method. S.M., L.C., and D.Y. performed the principal data analysis. J.W. performed the 3D reconstructions and contributed to the rugosity measures. J.D.C. contributed to the mechanical and electrical design of the CUREE camera array. T.A.M. provided the ecological insights that guided the work. Y.G. is the lead principal investigator (PI) of the project funding this work; contributed to the theoretical problem formulation; developed the original vision for the CUREE system; and supervised the engineers, students, and postdocs involved. S.M. and T.A.M. are co-PIs on the project. All authors contributed to the field experiments on St. John. **Competing interests:** The authors declare that they have no competing interests. **Data, code, and materials availability:** All data needed to support the conclusions of this manuscript are included in the main text or Supplementary Materials. Data are available on Zenodo at 10.5281/zenodo.16995714. Data processing and analysis code can be found at https://gitlab.com/whoi-smart-lab/papers/science_robotics_2025. No new materials were generated in this study.

Submitted 23 April 2025
Accepted 16 April 2026
Published 13 May 2026
10.1126/scirobotics.adx9939

Science Robotics

Autonomous seeking and mapping coral reef biodiversity hotspots with a multimodal AUV

Seth McCammon, Levi Cai, Daniel Yang, John Walsh, John D. Cast, T. Aran Mooney, and Yogesh Girdhar

Sci. Robot. **11** (114), eadx9939. DOI: 10.1126/scirobotics.adx9939

Science Robotics (ISSN 2470-9476) is published by the American Association for the Advancement of Science. 1200 New York Avenue NW, Washington, DC 20005. The title *Science Robotics* is a registered trademark of AAAS.